Mapping mean total annual precipitation in Belgium, by investigating the scale of topographic control at the regional scale.

Meersmans, J.[1*], Van Weverberg, K.[2], De Baets, S.[1], De Ridder, F.[3] , Palmer, S.J. [1], van Wesemael, B.[4], Quine, T.A.[1]

[1]University of Exeter, College of Life and Environmental Science, Department of Geography

[2]Met Office, Exeter, United Kingdom

[3]Flemish Institute for Technological Research (VITO), Energy & Technology

[4]Université catholique de Louvain, Georges Lemaitre Center for Climate Research, Earth and Life Institute, Louvain-la-neuve, Belgium

*corresponding author; e-mail: j.meersmans@exeter.ac.uk, Tel: +44(0)1392.72.44.88, Fax: +44(0)1392.72.33.42

Abstract

Accurate precipitation maps are essential for ecological, environmental, element cycle and hydrological models that have a spatial output component. It is well known that topography has a major influence on the spatial distribution of precipitation and that increasing topographical complexity is associated with increased spatial heterogeneity in precipitation. This means that when mapping precipitation using classical interpolation techniques (e.g. regression, kriging, spline, inverse distance weighting,…), a climate measuring network with higher spatial density is needed in mountainous areas in order to obtain the same level of accuracy as compared to flatter regions. In this study, we present a mean total annual precipitation mapping technique that combines topographical information (i.e. elevation and slope orientation) with average total annual rain gauge data in order to overcome this problem. A unique feature of this paper is the identification of the scale at which topography influences the precipitation pattern as well as the direction of the dominant weather circulation. This method was applied for Belgium and surroundings and shows that the identification of the appropriate scale at which topographical obstacles impact precipitation is crucial in order to obtain reliable mean total annual precipitation maps. The dominant weather circulation is determined at 260°. Hence, this approach allows accurate mapping of mean annual precipitation patterns in regions characterized by rather high topographical complexity using a climate data network with a relatively low density and/or when more advanced precipitation measurement techniques, such as radar, aren't available, for example in the case of historical data.

Keywords: precipitation, interpolation, weather circulation, slope, altitude, topography

1. Introduction

Precipitation is widely recognised as an important factor controlling environmental processes and therefore forms an essential input variable in many applications aimed at predicting or investigating these processes. Some of these applications, such as models predicting avalanches or landslides (Nolin & Daly, 2006; Van Den Eeckhaut, M., 2006) require both the temporal and spatial scale of the input precipitation fields to be very detailed. Other applications, in contrast, such as regional land use models, biogeochemical cycle models (e.g. carbon storage) or models of the co-evolution of mountain ranges and climate systems only require very detailed spatial scales, while fairly coarse monthly or even annual temporal scales are sufficient (e.g. Daly et al. 1993; Kittel et al., 1997; Roe and Baker 2006, Milne et al. 2007; Meersmans et al. 2012).

Recent studies (e.g. Parsons and Foster 2011) have suggested that the spatial variability of long-term average precipitation might be fairly large even at a within field/(sub)catchment level (resolution < 1 km), consequently questioning the use of anthropogenic radionuclide Cesium (^{137}Cs), i.e. globally deposited following atmospheric nuclear-bomb tests in the past (mainly 1950-1960's), as a proxy for erosion (Parsons and Foster 2011). Hence, identification of the resolution at which topography influences the spatial distribution of precipitation will be essential to evaluate the validity of commonly used precipitation fallout related radionuclide proxies (such as ^{137}Cs) at the landscape scale. One of the main reasons for the very large spatial variability of precipitation is its strong dependence on the terrain altitude and steepness as well as the orientation of the slopes. The literature indicates that even low elevation macro-relief structures can exhibit a significant effect on surface precipitation rates (e.g. Minder et al. 2008). An extensive review of the physical mechanisms

67 leading to larger precipitation amounts over terrain has been given recently by for example Roe
68 (2005) and Houze (2012). Houze (2012) describes at least two distinct mechanisms that could lead a
69 pre-existing frontal cloud to be enhanced and produce a precipitation maximum on the upwind side
70 of a low barrier. Firstly, the terrain could facilitate the gradual rise of warm air ahead of frontal
71 systems, while at the lee side of the hill the precipitating capacity is weakened by the down-slope air
72 motion (Houze, 2012). Secondly, the feeder-seeder mechanism could enhance precipitation rates
73 onto a ridge. In this case, an upper-level cloud (the feeder) is producing precipitation, while a low,
74 shallow, orographically-induced cloud (the seeder) could act to enhance the precipitation by
75 accretion of the cloud droplets onto the precipitating particles from the cloud above. During
76 summer, convective events also contribute significantly to the total rainfall in the region of interest
77 (Roe, 2005). Convective events might be affected by low terrain in various ways, e.g. by triggering by
78 lee-waves in the wake of a hill (Houze, 2012). By the mechanism listed above, low elevation barriers
79 do have the potential to influence the dominant weather circulation and, therefore, could exercise a
80 primary control on the regional spatial precipitation pattern in these environments.

81

82 Despite the widely recognised importance of the spatial distribution of precipitation over complex
83 terrain, many regional climate inventories are based on long term observations from sparse
84 meteorological stations. For example, relatively coarse precipitation maps are available at the
85 national or continental scale, from the ATEAM project (Mitchell et al., 2004). Most often, point data
86 are extrapolated to a continuous grid by using classical interpolation techniques, such as nearest
87 neighbor methods, local linear regression, inverse distance weighting, spline or kriging methods
88 (without or with external drift) (e.g. Goovaerts, 2000; Lloyd, 2005; Daly, 2006; Basistha et al. 2008;
89 Tobin et al. 2011). In most cases these techniques are not satisfactory, since the spatial
90 heterogeneity of precipitation and their resolutions are sub-optimal for ecological and environmental
91 modelling. Mapping precipitation in regions characterized by complex topography, such as

mountainous regions, demands higher density measurements in order to obtain a climate map with a spatially uniform quality level when using classical interpolation techniques (Daly, 2006). Nevertheless, the cost of monitoring at sufficient density may be prohibitive and there is, therefore, a need to develop strategies for interpolation of data that capture the structure of precipitation patterns, which will help in setting-up more efficient monitoring networks.

This has lead over the last decades to increased efforts in developing techniques to obtain a more accurate interpolation, based on elevation data (e.g. Sen and Habib 2000, Lloyd 2005, Di Luzio et al. 2008, Gottardi et al. 2012) or using the slope orientation of mountain ranges (e.g. Turner et al. 2009, Hughes et al. 2008). One of the most promising approaches to the characterisation of topographic control on spatial patterns of precipitation is the Precipitation-elevation Regressions on Independent Slopes Model (PRISM) (e.g. Daly et al. 2002). In this model precipitation is interpolated for each grid cell of the digital elevation model (DEM) based on a simple weighted precipitation-elevation regression with distance to station, coastal proximity, general slope orientation and vertical layer (inversion layer or not) as weighting factors. In the application of PRISM, it is critical to understand at which scale precipitation is influenced by the topography. Daly et al. (2002) explored this question using 6 DEMs with a differing smoothing level, based on station data density and local terrain complexity.

Even more advanced techniques combine information obtained from weather radar with that from rain gauges. Goudenhoofdt and Delobbe (2009) showed that a recent technique based on the geostatistical merging of weather radar and rain gauges provides spatially and temporally accurate daily rainfall accumulation predictions. While this approach certainly has the potential to improve our understanding of the relation between topography and precipitation, the fairly recent advent of

116 weather radars prohibits the application of this approach to historical data, long time periods or
117 regions not covered by weather radar.

118

119 Hence, there is still a need for interpolation techniques of intermediate complexity to obtain
120 reasonable estimates of surface precipitation with high spatial resolution, only based on information
121 from rain gauges and terrain characteristics. One of the main caveats with techniques like PRISM, is
122 that it is not known a priori what the optimal scale is of the input fields. In addition, information on
123 the prevailing rain-bearing wind direction could be a significant improvement to PRISM. To
124 overcome this shortcoming, recently Gottardi et al. (2012) conducted a novel methodology to map
125 daily precipitation amounts in main mountain ranges in France (i.e. Pyrenees, Central Massif and
126 Alps) by combining a local elevation–precipitation model (comparable to PRISM) with a weather
127 pattern classification. They defined 8 different weather patterns (e.g. Southwest circulation or
128 anticyclonic) and an associated linear orographic precipitation gradient. The gridded precipitation
129 was a function not only of elevation, but also of the weather-pattern specific gradient, giving weights
130 to neighbouring stations using a "crossing distance" and taking into account crests and valleys
131 between the stations and the grid cell of interest. While this method provides very detailed daily
132 estimates of surface precipitation, it is also computationally expensive, given the identification of the
133 weather pattern for each day.

134

135 This study discusses a novel, computationally affordable interpolation technique, using the
136 dominant rain-bearing wind direction and the optimal scales of topographical variables, aimed
137 specifically at regions with sparse data over terrain with intermediate complexity or to reconstruct
138 very detailed historical precipitation maps. The scale at which relief influences precipitation will be
139 investigated, and the direction of the dominant weather circulation identified. These two

components form essential elements in the present novel spatial precipitation model approach, which will help us to support the hypothesis of the existence of a rain shadow effect in these environments. More specifically, this methodological framework will be applied to a specific case study, i.e. predicting average yearly precipitation (1960-1990) in Belgium and surroundings, including the Ardennes – Eifel massif situated at the Belgian- German border (Fig. 1).

2. Material and methods

2.1. Study area

The northern and western parts of Belgium are situated in the North-west European lowlands and are characterized mainly by altitudes less than 100 meters above sea level. The Ardennes-Eiffel massif covers the eastern and southern part of the study area and reaches altitudes up to 700 meters (Fig. 1-A). The study area is characterized by a temperate maritime climate, with a mean annual temperature and total annual precipitation amounts ranging from about 10°C and 700 mm in the west to about 6°C and 1400 mm in the southeast.

Figure 1-B shows that the 30-year average annual precipitation amounts of the stations in Kall (860 mm yr^{-1}) and Nuerburg (872 mm yr^{-1}), situated in the eastern part of the Ardennes - Eiffel massif at altitudes of respectively 550 and 629 m asl, are remarkably low compared to the stations near the summit and/or situated on the western part at similar or even lower altitudes (e.g. La Gleize:1212

mm yr^{-1} at 412 m asl, Eupen Ternell: 1326 mm yr^{-1} at 565 m asl, Mont Rigi: 1450 mm yr^{-1} at 680 m asl). Furthermore, the 30-year average annual precipitation amount in Mayen (230 m asl.) at 596 mm yr^{-1} is remarkably low. This station is situated in the most eastern part of the Ardennes – Eiffel massif and so probably very well shielded from east – west precipitation supply by the configuration of the mountain range. This clearly shows the existence of a rain shadow effect.

2.2. Climate and Topographical data

Mean long-term climate data for the period 1961-1990 were obtained for Belgian stations from the 'Koninklijk Meteorologisch Instituut (KMI)', for the Southern part of The Netherlands from the 'Koninklijk Nederlands Meteorologisch Instuut (KNMI)', for West Germany from the 'Deutscher Wetterdienst (DWD)' and for North France from 'Meteo France'. In total 201 meteorological stations, with a good geographical spread, were selected for the analysis (fig. 1-A).

The "SRTM Digital Elevation Data" distributed by "The CGIAR Consortium for Spatial Information (CGIAR-CSI)" with a resolution of 90 meters and produced by the NASA originally, were used as topographical source data (The CGIAR Consortium for Spatial Information, 2008).

2.3. Precipitation model

'Altitude' and 'deviation of the orientation of the slope to the orientation of the dominant weather circulation' were selected as input variables for the model. The orientation of the dominant rain-

bearing weather circulation in the study area is from the west, as shown by e.g. Brisson et al. (2011). This is because all vast water bodies (i.e. North Sea and Atlantic Ocean) are situated in the west, and hence the dominant westerly winds at this latitude advect relative humid maritime air. This implies that under this assumption the 'deviation of the orientation of the slope to the ODWC' will express the angle between the west and the orientation of the slope. So under the assumption that west is the direction of the dominant weather circulation, the more the slope orientation deviates from the west, the higher this value will be. For example, north and south oriented slopes are characterized by a value of 90°, while east oriented slopes have a value of 180°.

Moreover, we note that the influence of slope orientation on precipitation strongly depends on its altitude above sea level. For example, seawards oriented slopes can influence the weather circulation more efficiently when they are situated at higher altitude. Consequently, the 'deviation of the orientation of the slope to the ODWC' variable is expressed in the final model as an interaction term with altitude (eq. 1).

$$prec = a.H_1 + b.H_2.S + c \quad (1)$$

where:

prec = long term (30 yrs) average annual precipitation amount (mm yr^{-1})

H_1 = height above sea level (m)

H_2 = height above sea level (m) in the interaction term

S = deviation of the orientation of the slope to the direction of the dominant weather circulation (ODWC)

206 a, b, c = model parameters

207

208 Note that the present model has been calibrated based on the 30-year average annual precipitation
209 amounts from the 201 meteorological stations, but subsequently, this calibrated model has been
210 applied in a spatial explicit way in order to obtain a precipitation map covering the entire study area.
211 Moreover, although the H1 and H2 variables in this model both represents the height above sea level
212 (either as a separate term or embedded in an interaction term), the associated values will most
213 probably be different as they can be abstract from different levels of topographical detail as obtained
214 after applying the present topographical smoothing procedure (see section 2.4 and fig. 2 for more
215 details).

216

217 2.4. Detection of the scale of topographical control and orientation of the dominant weather
218 circulation

219

220 As this study aims to detect the scale at which low elevation topographical barriers within the study
221 area impact the spatial distribution of mean total annual precipitation, the present model's (eq. 1)
222 performance was investigated using a wide range of input variable maps (H_1, H_2, S), reflecting
223 different degrees of spatial heterogeneity. This allowed us to identify the optimal level of
224 topographical detail of these variables in order to map mean total annual precipitation over the
225 entire study area. In addition, the detection of the ODWC is another important element in the
226 present methodology. Hence, the above made assumption of west as ODWC will be tested and
227 refined if needed. A detailed description of the associated methodological approach can be found
228 below, and a schematic overview is provided in figure 2.

229

230 After converting the original DEM into maps presenting the deviation of the slope towards 19
231 different potential ODWCs, i.e. every 10° between South (180°) and North (360°), the model's
232 topographical input maps (H_1, H_2, S) were aggregated to different spatial resolutions. In total, 80
233 different levels of aggregation were considered, resulting in a set of maps ranging in resolution from
234 90 meters to 103.5 kilometers for each of the input variables. The resulting aggregated input maps
235 were smoothed to remove unrealistically sharp gradients before running the model and producing
236 spatial predictions. While all model input maps were resampled to a resolution of 90 meters during
237 the smoothing procedure, it is important to note that the same level of detail is maintained (i.e.
238 determined by the aggregated map prior to smoothing). This allowed us to use continuous input
239 maps and therefore make more realistic spatial model predictions. After comparing the performance
240 of two commonly used interpolation techniques (i.e. "Spline" and "Natural Neighbor", e.g. Lam
241 (1983)) for both "Altitude" and "Deviation of the orientation of the slope towards the West", our
242 analysis led us to use "Spline" to smooth H_1 and H_2 and "Natural Neighbor" to smooth S model input
243 maps (Fig. 3). For each of the 9,728,000 combinations of smoothed H_1, H_2 and S input maps,
244 corresponding topographical values for all the meteo-stations were derived from the maps and the
245 model (eq. 1) was applied to estimate 30-year average annual precipitation amounts (mm yr^{-1}).

246

247 For each potential ODWC, a combination of the H_1, H_2 and S maps with the highest determination
248 coefficient (R^2), was selected and compared to detect a more accurate ODWC. The finally selected
249 model output (i.e. with the overall highest R^2) was combined with associated H_1, H_2 and S maps at
250 corresponding resolutions in order to produce a 30-year average annual precipitation (mm yr^{-1}) map
251 for Belgium.

252

2.5. Cross Validation

In addition, for every potential ODWC, a repeated 10-fold cross validation procedure was carried out (1000 replicates) on each best model fit (i.e. map resolutions with highest R^2). Thereby, 90% of the data was randomly chosen for calibration and 10% for validation as it is commonly recommended (Hastie et al. 2001). By comparing the predicted and observed values of the validation samples Root Mean Square Error (RMSE, eq. 2) and Ratio of Performance to Deviation (RPD, eq. 3) of the model were calculated. The latter expresses how many times the predictive ability of the model is stronger than just using the average precipitation value. In other words, RPD values of 2, 3 and 4 mean that respectively 50%, 66.67% and 75% of the total variation in the validation dataset is captured by the model.

$$RMSE = \sqrt{\frac{1}{n}.\sum_{i=1}^{n}(P_{obs(i)} - P_{pred(i)})^2} \quad (2)$$

Where RMSE is Root Mean Square Error (mm yr^{-1}), n is overall number of samples used in the validation procedure, $P_{obs(i)}$ is the observed value of i^{th} 30-year average annual precipitation measurement (mm yr^{-1}) and $P_{pred(i)}$ is the predicted value of i^{th} 30-year average annual precipitation measurement (mm yr^{-1}).

$$RPD = \frac{STD}{RMSE} \quad (3)$$

With RPD being the ratio of performance to deviation and STD is standard deviation of all total yearly precipitation measurements (mm yr^{-1}).

3. Results & Discussion

3.1. Topographical smoothing

In figure 3 the performances of the interpolation techniques “Spline” and “Natural Neighbor” in order to smooth “altitude” and “deviation of the orientation of the slope to the West” maps were analysed. This was based on RMSE-output obtained by comparing the basic topographical data (i.e. SRTM – DEM derived) at a resolution of 90 meters with a range of smoothed maps, i.e. at corresponding aggregation resolution levels of 0.45km, 0.9km, 4.5km, 9km, 45km, 90km, considering 3 different height classes (i.e. < 200m; 200-400m and > 400m). These results show that Spline is the best interpolation method when smoothing the altitude (H_1, H_2, eq. 1) maps (i.e. lowest RMSE), at least when considering height classes < 200m and > 400m. No clear differences have been found for the 200-400 m height class. On the contrary, when considering the “deviation of the orientation of the slope to the West” Natural Neighbor seems to be the best interpolation method, with lower RMSE values than Spline for all altitude classes. Moreover, it’s important to note that Spline returns values out of the theoretical possible range of 0°-180°, which is an additional reason why Natural Neighbor is the most appropriate interpolation technique to be used when smoothing the “deviation of the orientation of the slope to the ODWC” (S, eq. 1) maps.

297 3.2. Model parameter identification and performance

298

299 Table 2 shows that the best model fit, i.e. with highest R^2, was obtained using the smoothed altitude
300 maps derived from aggregated DEMs with a resolution of 8.1 and 90 kilometers, for respectively H_1
301 and H_2 (eq. 1), and a "deviation of the orientation of the slope to 260° (i.e. the orientation of the
302 dominant weather circulation, ODWC) map" with a resolution of 30.6 kilometers. This model fit has
303 an R^2 value of 0.82 and all estimated parameters are significant ($p<0.05$) (table 1). Table 2 shows an
304 overview of the top 10 of best model fits, ranked based on R^2, with annotation of ODWC and
305 aggregation resolution of smoothed model input maps (H1, H2 and S (eq. 1)). It is remarkable that
306 within this top 10 of best model runs (with R^2 values ranging between 0.8149 and 0.8192), there is
307 only limited variation in ODWC and aggregation resolution of smoothed model input maps. For
308 example besides 6 model fits with an ODWC of 260°, 4 model fits have an ODWC of 270°, which may
309 suggest that more precisely the ODWC is situated somewhere in between 260° and 270°. Figure 4
310 shows the determination coefficients of the different model runs as function of the aggregation
311 resolution of the smoothed DEM (H1 and H2) and S maps including the selected best model run at R^2
312 = 0.82. The trendlines in these figures are a combination of a power and exponential law. It is
313 interesting to note that for variable H_1, an additional linear term was required to fit the distribution,
314 especially the very low R^2 values at lower resolutions, indicating the importance of the term of
315 variable H_1 in the model as well as the selection of the appropriate level of spatial detail of these
316 variables. Despite the fact that 8.1 km has been identified as the most appropriate aggregation
317 resolution of H_1 input maps, the trendline (reaching its max. value at a resolution of 4.5 km) indicates
318 that using an H_1 map with a finer resolution (i.e. within the 4-8 km resolution range) seems to be a
319 valuable option as well (Fig 4a). The range of potentially useful aggregation resolutions of maps
320 representing the variables in the interaction factor is wider with roughly 50-100 km for H_2 (i.e.
321 trendline's max. value at 70.8 km, Fig. 4b) and 20-40 km for S (i.e. trendline's max. value at 30.2 km,

322 Fig. 4c). In addition the range of R^2 values covered by these variables (i.e. 0.64-0.82) shows that
323 including the interaction factor in the model instead of simplified version whereby precipitation is
324 only predicted as a linear function of altitude, results in a significant improvement of the R^2 with 0.18
325 (Fig. 4b,c). Moreover, the model cross-validation shows a root mean square error (RMSE) of 66.0 mm
326 yr^{-1} and ratio of performance to deviation (RPD) of 2.33. Figure 5 illustrates RMSE and RPD values of
327 the H1, H2 and S maps combination with the maximal R^2 as a function of orientation of the dominant
328 weather circulation. The results show that the selected best model fit has the best validation
329 statistics, i.e. lowest RMSE and highest RPD, and underlines that the dominant weather circulation in
330 Belgium is most probably at or very close to 260°.

331

332 The precipitation map we derived (figure 6) shows that precipitation increases with increasing
333 altitude (Fig. 6). Furthermore, as this study detects a ODWC at an aspect of 260° for the study area,
334 the Ardennes – Eiffel massif is influenced by a mainly west-east oriented weather circulation,
335 resulting in higher precipitation amounts at the western side of the Ardennes massif (Belgium)
336 compared to the eastern side (Eiffel - Germany) (Fig. 6). To detect this effect one should consider the
337 macro relief structure of the topographical barrier. These findings underline the importance of the
338 influence of lower elevation relief units on the spatial distribution of precipitation patterns and
339 clearly show orographic precipitation and the existence of a rain shadow effect, i.e. in this particular
340 study, in the western and the eastern parts of the Ardennes-Eiffel massif, respectively. Furthermore,
341 the model predicts that smaller topographical barriers (i.e. mostly north-south oriented relief units
342 with dimensions between 10 and 50 kilometers) have an influence on spatial distribution of
343 precipitation as well, such as the north-south oriented cuestas in the North-east of France (A) and
344 the plateau in the eastern part of Limburg (north-east Belgium, B) or as indicated by the higher
345 precipitation values in the Condroz region (C) as compared to Fagne-Famenne depression (D) (Fig. 1
346 and 6).

In general, relative errors are restricted and in most areas to below 10% (Fig. 6). No clear dominant regional pattern error can be detected. Nevertheless most important relative errors are found in the western part of the Ardennes-Eifel massif, characterized by high precipitation amounts, with more precisely a clear local underprediction in the South - Southwest and Northwest (I) and an overprediction in central (II) parts of this particular region. Furthermore, one can observe a general tendency of overprediction east of the Eifel (i.e. Mosel and Rhine Valley (III), as well as in the most western part of Belgium and Northwest of France (IV) and an underprediction in the North of Belgium (V) as well is in the Northeastern corner of the study area (VI) (Fig. 5).

The present precipitation mapping method answers two important questions:

1) at which scale does topography influence the spatial pattern of precipitation? and

2) what is the orientation of the dominant weather circulation (ODWC)?

In comparison to classical interpolation techniques, it allows accurate mapping in regions characterized by high topographical complexity without the need of a dense measuring network. Moreover, as the input data is restricted, i.e. a rather coarse DEM (e.g. SRTM 90m covering entire world and free available) and climate data at common measurement density, we believe that the method has great potential to be applied in other regions characterized by a comparable topographical complexity in order to improve particular spatial prediction of the precipitation pattern. In addition, as the present method is based on a simple formula, it has the advantage of being a computationally 'low-cost' approach, increasing its applicability, especially as compared to other recently developed advanced precipitation interpolation methods (e.g. Gottardi et al. 2012)

where for each spatial-temporal unit (pixel / day), a calibration procedure needs to be carried out. A simplified version of the present model (i.e. without ODWC detection component) has been recently applied successfully in a study conducting a spatial and temporal analysis of soil organic carbon in Belgium (Meersmans et al. 2011), underlining the need of detailed precipitation maps (and mapping methods) as essential input information for accurate spatial prediction of (soil) key environmental parameters. Furthermore, it is important to notice that the present methodology complements more advanced techniques, making use of radar and providing spatial information of precipitation at very fine spatial and temporal scales (Goudenhoofdt and Delobbe, 2009). This is especially relevant for regions with a high topographical complexity, but characterized by sparse climatological data network and/or when the aim is to map historical precipitation data (i.e. when radar was not yet available or for averages over longer periods in time). Finally, the fact that 8, 36 and 90 kilometer are identified as the optimum scales at which topography influences precipitation (respectively for H1, S and H2 (see eq. 1)), seems to reject Parsons and Foster`s (2011) concern regarding the use of ^{137}Cs as a proxy for erosion due to a potential significant variation in fallout by precipitation at the within field scale (i.e. at resolutions below 1 kilometer). Nevertheless, it should be stressed that we identified the optimal scales for the topography for this region specifically, and therefore, it is probable that these optimal scales might be different for other regions in the world characterized by different a degrees of terrain complexity or macro meteorological settings, such as more alpine environments.

3.3. Comparison against Kriging

As previous studies have illustrated the high potential of using advanced geostatistical methods such as kriging to interpolate mean annual and seasonal precipitation amounts at the regional scale,

underlining the importance of the existence of a significant spatial autocorrelation in the data (e.g. Dingman et al., 1988; Goovaerts, 2000; Masson and Frei, 2014), we have (i) evaluated if the predicted precipitation amounts obtained by the presented model preserved the spatial variability of the underlying observations; and (ii) made a comparison between the precipitation maps obtained with the model presented in this study and by applying Ordinary Kriging.

Figure 7 compares the semivariograms, as produced by ARC-GIS' Geostatistical Wizard tool, from the observed data and the model predicted values. Although this figure shows that the average semivariance (see e.g. Goovaerts (2000) for equation) at any given distance between points is slightly lower in the case of the estimated values as compared to the original data, the nugget, range and sill are rather comparable considering both the Spherical and Gaussian model fits. When comparing predicted against observed values, the range is 20% and 15% higher, while the sill is 12% and 8% lower, for the Spherical and Gaussian model fits respectively (Fig. 7). These results indicate that the model output preserves to a large extent the spatial variability of the precipitation data.

The comparison of the spatial patterns in precipitation obtained by the approach presented in this study (Fig. 8a) with Ordinary Kriging (Fig 8b), shows that Ordinary Kriging produces a much less detailed image in the more topographical complex zone in the Eastern part of the study area (i.e. along the Ardennes-Eifel massive) in comparison to the approach presented in this study (Fig. 8a-b). In contrast, in the Northern and Western parts of the study area, where no significant topographical features are present, Ordinary Kriging predicts a larger spatial variability in precipitation as compared to our approach (Fig. 8a-b). In addition, although the relative differences between both precipitation maps are generally larger than the relative model errors (bias) of the present approach (i.e. typically below 30% and 10%, respectively (Fig. 8c)), a spatial correlation exists between both. More precisely,

418 precipitation values are generally higher for this study's modelled precipitation map compared to the
419 map generated with Ordinary Kriging in areas in which the model is characterized by a regional
420 overall trend of over-predictions (II, III & IV, Fig. 6 & 8c). In areas in which the model is characterized
421 by a regional overall trend of under-prediction (I, V & VI Fig. 6& 8c), precipitation values are
422 considerably lower on this study's map compared to the map created by Ordinary Kriging. This
423 indicates the largely complementary character of both methodologies, as it seems that Ordinary
424 Kriging may have the potential to compensate for regional under/over predictions made by the
425 presented model. Hence, one can conclude that there exists a scope for future research in which
426 both interpolation methods could be combined in order to improve the overall performance of
427 rainfall predictions in this or similar study areas. Another potential future avenue of research can
428 be the application of the presented model at smaller temporal scales such as seasonal or monthly
429 averaged total rainfall amounts.

430

431 4. Conclusion

432

433 This study shows that long term mean annual precipitation amounts are strongly influenced by
434 topography in lower elevation relief structures and offers a simple methodology to map
435 climatologically averaged precipitations patterns in these regions when lacking a dense
436 meteorological measuring network. Mean annual precipitation can be modelled as a function of
437 smoothed altitude and slope orientation maps. Best results were obtained using smoothed altitude
438 maps at aggregation resolutions of 8.1km and 90 km (i.e. outside (H_1) and within interaction term
439 (H_2) of the model (eq. 1), respectively) and a smoothed slope orientation map showing a deviation of
440 the slope orientation to the north aspect of 260°, indicating the orientation of the dominant weather
441 circulation (ODWR), at aggregation resolution of 30.6 km. The resulting precipitation map shows

clearly that the Ardennes – Eiffel massif range determines, to a large extent, the spatial distribution of total yearly precipitation amount in the region. As this lower elevation relief units block precipitation supply from dominant west – east weather circulations, the western part of this topographical barrier receives remarkably higher precipitation amounts than the eastern side situated in the rain shadow of this mountain range. Furthermore, given the limited need for input data, this method is easily applicable to other regions. Hence, the method has a large potential to improve the interpolation of spatial patterns of precipitation in mountainous regions, characterized by a sparse data network and/or when more modern and advanced techniques, such as weather radars, are not available.

5. Acknowledgement

We are grateful to the national meteorological institutes of Belgium (Koninklijk Meteorologisch Instituut (KMI)), France (Meteo France), The Netherlands (Koninklijk Nederlands Meteorologisch Instuut (KNMI)) and Germany (Deutscher Wetterdienst (DWD)) for providing the data. In addition we thank the two anonymous reviewers, whose comments resulted in significant improvements to the manuscript.

6. References

464 Basistha, A., Arya, D.S., Goel, N.K., 2008. Spatial distribution of rainfall in Indian Himalayas – A case
465 study of Uttarakhand region, Water Resources Management, 22, 1325-1346.

466

467 Brisson, E., Demuzere, M., Kwakernaak, B., van Lipzig, N.P.M, 2011. Relations between atmospheric
468 circulation and precipitation in Belgium. Meteorology and Atmospheric Physics, 111, 27-39.

469

470 Daly, C., Neilson, R.P., Philips, D.L., 1993. A statistical-topographical Model for Mapping
471 Climatological Precipitation over Mountainous Terrain. Journal of Applied Meteorology. 33, 140-158.

472

473 Daly, C., Wayne, G.P., Taylor, G.H., Johnson, G.L., Pasteris, P., 2002, A knowledge-based approach to
474 the statistical mapping of climate. Climate Research, 22, 99-103.

475

476 Daly, C., 2006. Guidelines for assessing the suitability of spatial climate data sets, International
477 Journal of Climatology, 26, 707-721.

478

479 Di Luzio, M., Johnson, G.L., Daly, C., Eischeid, J.K., Arnold, J.G., 2008. Constructing Retrospective
480 Gridded Daily Precipitation and Temperature Datasets for the Conterminous United States. Journal of
481 Applied Meteorology and Climatology, 47, 475-497.

482

483 Dingman, S.L., Seely-Reynolds, D.M, Reynolds, R.C. 1988. Applications of kriging to estimating mean
484 annual precipitation in a region of orographic influence. Water Resources Bulletin. 24, 329-339.

485

486 Goovaerts, P., 2000. Geostatistical approaches for incorporating elevation into the spatial
487 interpolation of rainfall. Journal of Hydrology. 228, 113-129.

488

489 Gottardi, F., Obled, C., Gailhard, J., Paquet, E., 2012. Statistical reanalysis of precipitation fields based
490 on ground network data and weather patterns. Applications over French mountains. Journal of
491 Hydrology, 432-433, 154-167.

492

493 Goudenhoofdt, E., Delobbe, L., 2009. Evaluation of radar-gauge merging methods for precipitation
494 estimates. Hydrology and Earth System Sciences, 13, 195-203.

495

496 Hastie, T., Tibshirani, R., Friedman, J., 2001. The Elements of Statistical Learning, Data Mining,
497 Inference, and Prediction, Second Edition, Springer Series in Statistics, Springer-Verlag, New York.

498

499 Houze, R.A., 2012. Orographic effects on precipitating clouds. Reviews of Geophysics, 50, doi:
500 10.1029/2011RG000365.

501

502 Hughes, M., Hall, A., Fovell, R.G., 2008. Blocking in areas of complex topography, and its influence on
503 rainfall distribution. Journal of the Atmospheric Sciences, 66, 508-518.

504

505 Kittel, T.G.F., Royle, J.A., Daly, C., Rosenbloom, N.A., Gibson, W.P., Fisher, H.H., Schimel, D.S.,
506 Berliner, L.M., 1997. A gridded historical (1985-1993) bioclimate dataset for the conterminous United
507 States. 10th Conference on Applied Climatology, 219-222.

508

509 Lam, N. S.-N. 1983. Spatial Interpolation Methods: A Review. The American Cartographer, 10, 129-
510 150.

511

512 Lloyd, C.D., 2005. Assessing the effect of integrating elevation data into the estimation of monthly
513 precipitation in Great Britain. Journal of Hydrology, 308, 128-150.

514

515 Masson, D., Frei, C. 2014. Spatial analysis of precipitation in a high-mountain region: exploring
516 methods with multi-scale topographic predictors and circulation types. Hydrology and Earth System
517 Science, 18, 4543-4563.

518

519 Minder, R.J., Durran, D.R., Roe, G.H., Anders, A.M., 2008. The climatology of small-scale orographic
520 precipitation over the Olympic Mountains: Patterns and processes. Quarterly Journal of the Royal
521 Meteorological Society, 134, 817–839.

522

523 Milne E., Al Adamat R., Batjes N.H., Bernoux M., Bhattacharyya T., Cerri C.C., Cerri C.E.P., Coleman K.,
524 Easter M., Falloon P., Feller C., Gicheru P., Kamoni P., Killian K., Pal D.K., Paustian K., Powlson D.S.,
525 Rawajfih Z., Sessay M., Williams S., Wokabi S., 2007. National and sub-national assessments of soil
526 organic carbon stocks and changes: The GEFSOC modelling system. Agriculture Ecosystems and

527 Environment, 122, 3-12.

528

529 Mitchell T.D., Carter, T.R., Jones, P.D., Hulme, M., New, M., 2004. A comprehensive set of high
530 resolution grids of monthly climate for Europe and the globe: the observed record (1901 2000) and
531 16 scenarios (2001 2100). Tyndall Centre working Paper, 55, University of East Anglia, Norwich,
532 United Kingdom.

533

534 Meersmans, J., van Wesemael, B., Goidts, E., Van Molle, M., 2011. Spatial analysis of soil organic
535 carbon evolution in Belgian croplands and grasslands, 1960-2006. Global Change Biology, 17, 466-
536 479.

537

538 Meersmans, J., Martin, M. P., Lacarce, E., De Baets, S., Jolivet, C., Boulonne, L., Lehmann, S., Saby, N.
539 P. A., Bispo, A., Arrouays, D., 2012. A high resolution map of French soil organic carbon. Agronomy
540 for Sustainable Development, 32, 841-851.

541

542 Nolin, A., Daly, C., 2006. Mapping "At Risk" Snow in the Pacific Northwest, Journal of
543 Hydrometeorology, 7, 1164-1171.

544

545 Parsons, A.J., Foster, I.D.L., 2011. What can we learn about soil erosion from the use of ^{137}Cs? Earth-
546 Science Reviews, 108, 101-113.

547

548 Roe, G.H., 2005. Orographic Precipitation. Annual Review of Earth and Planetary Sciences, 33, 645-
549 671.

550

551 Roe, G.H., Baker, M.B., 2006. Microphysical and geometrical controls on the pattern of orographic
552 precipitation. American Meteorological Society, 63, 861-880.

553

554 Sen, Z., Habib, Z., 2000. Spatial precipitation assessment with elevation by using point cumulative
555 semivariogram techniques. Water resources management, 14, 311-325.

556

557 The CGIAR Consortium for Spatial Information, 2008. SRTM Digital Elevation Data,
558 http://srtm.csi.cgiar.org/

559

560 Tobin, C., Nicotina, L., Parlange, M.B., Berne, A., Rinaldo, A., 2011. Improves interpolation of
561 meteorlogical forcings for hydrologic applications in a Swiss Alpine region. Journal of Hydrology, 401,
562 77-89.

563

564 Turner, J., Connolley, W. M.., Leonard,S., Marshall, G.J and Vaughan, D.G., 2009. Spatial and temporal
565 variability of net snow accumulation over the Antarctic from ECMWF re-analysis project data.
566 International Journal of Climatology, 19, 697-724.

567

568 Van Den Eeckhaut, M., Vanwalleghem, T., Poesen, J., Govers, G., Verstraeten, G., Vandekerckhove, L.,
569 2006. Prediction of landslide susceptibility using rare events logistic regression: a case-study in the
570 Flemish Ardennes, Belgium, Geomorphology, 76, 392–410.

571

572

7. Figures

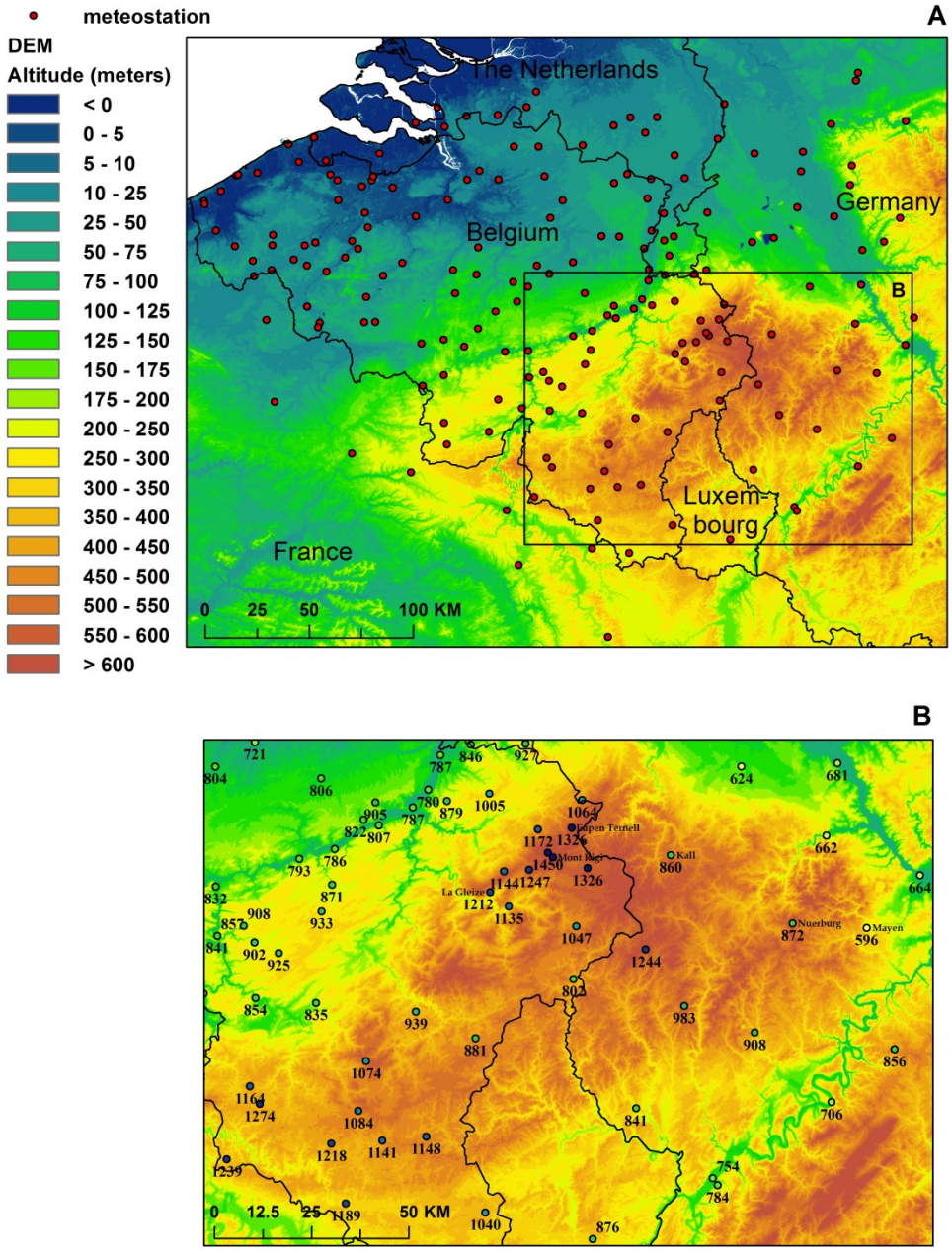

Figure 1: A) Localization of the 197 selected meteostations on the SRTM-DEM with a resolution of 90m in and around Belgium. B) Annotation of the measured 30-year average annual precipitation amounts (mm yr^{-1}) of the local meteostations along the Ardennes - Eiffel massif.

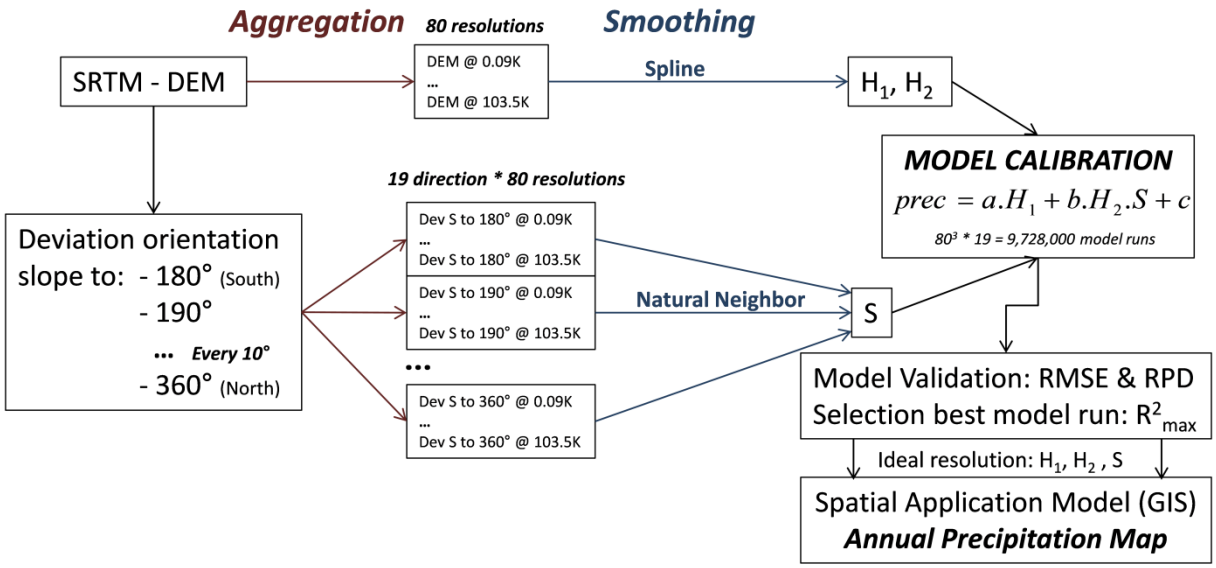

580

581 Figure 2: Methodological Flowchart

582

583

584

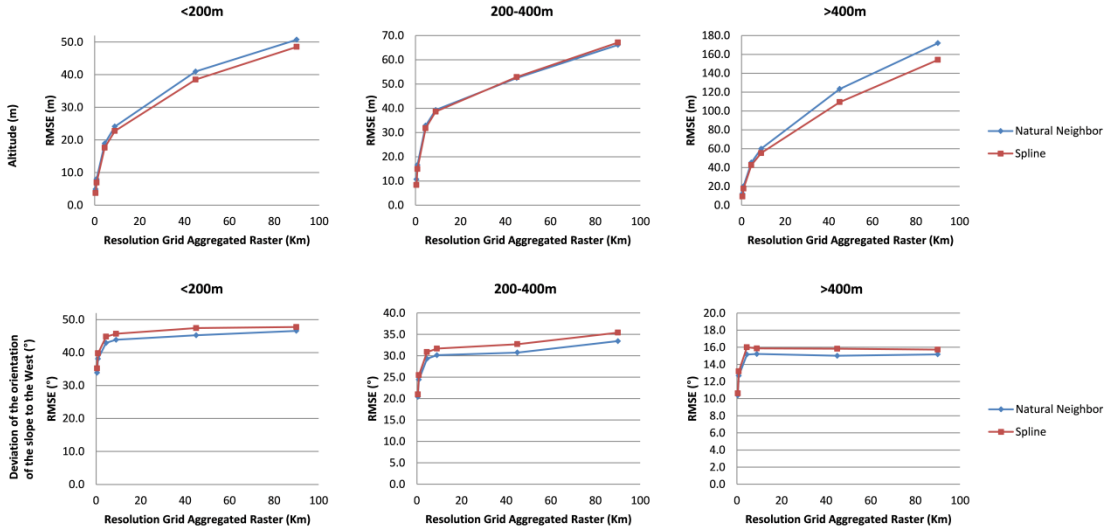

585

586 Figure 3: Comparison of interpolation techniques “Spline” and “Natural Neighbor” used to smooth

587 aggregated model input maps of Altitude and “Deviation to the orientation of the slope to the West”

588 at 3 different altitude intervals (< 200 meters, 200-400 meters, > 400 meters)

589 .

590

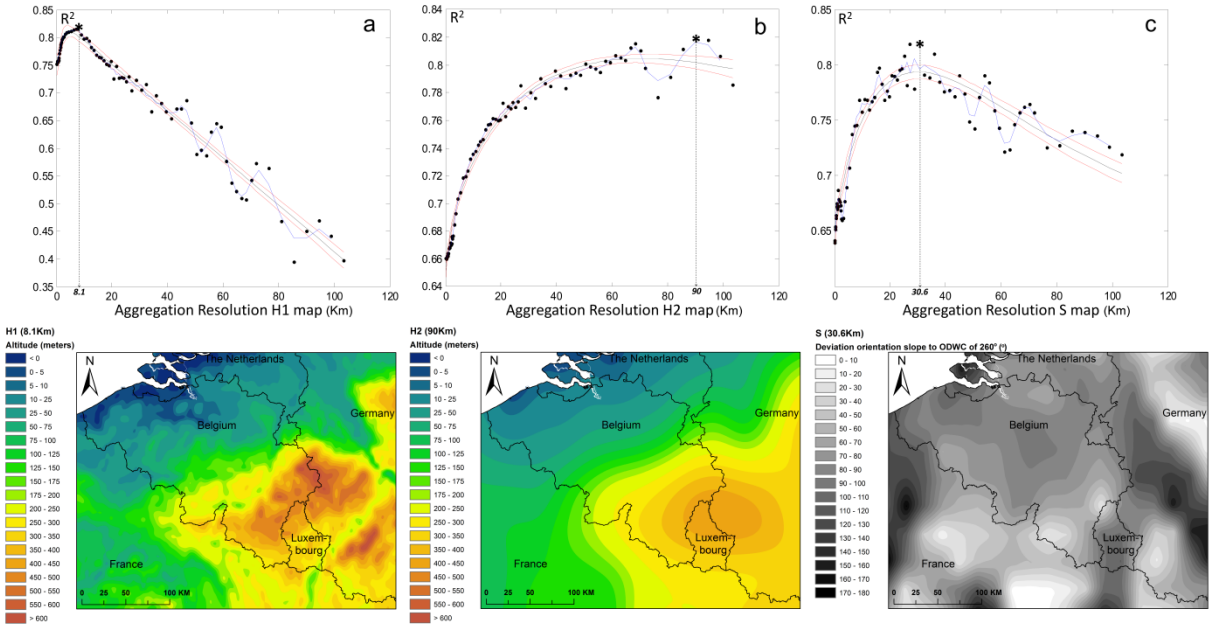

591

592 Figure 4: Determination coefficients (R^2) of the different precipitation model runs as a function of the
593 resolution of the aggregation level of the altitude input maps (km), i.e. a) H_1 and b) H_2 (eq. 1), and
594 deviation of the orientation of the slope to the dominant weather circulation (260°) maps, i.e. c) S
595 (eq.1), including the selected best model run as indicated by * (R^2_{max} = 0.8192) as well as presentation
596 of associated input maps (i.e. H_1 at 8.1 km; H_2 at 90 km and S at 30.6 km)

597

598

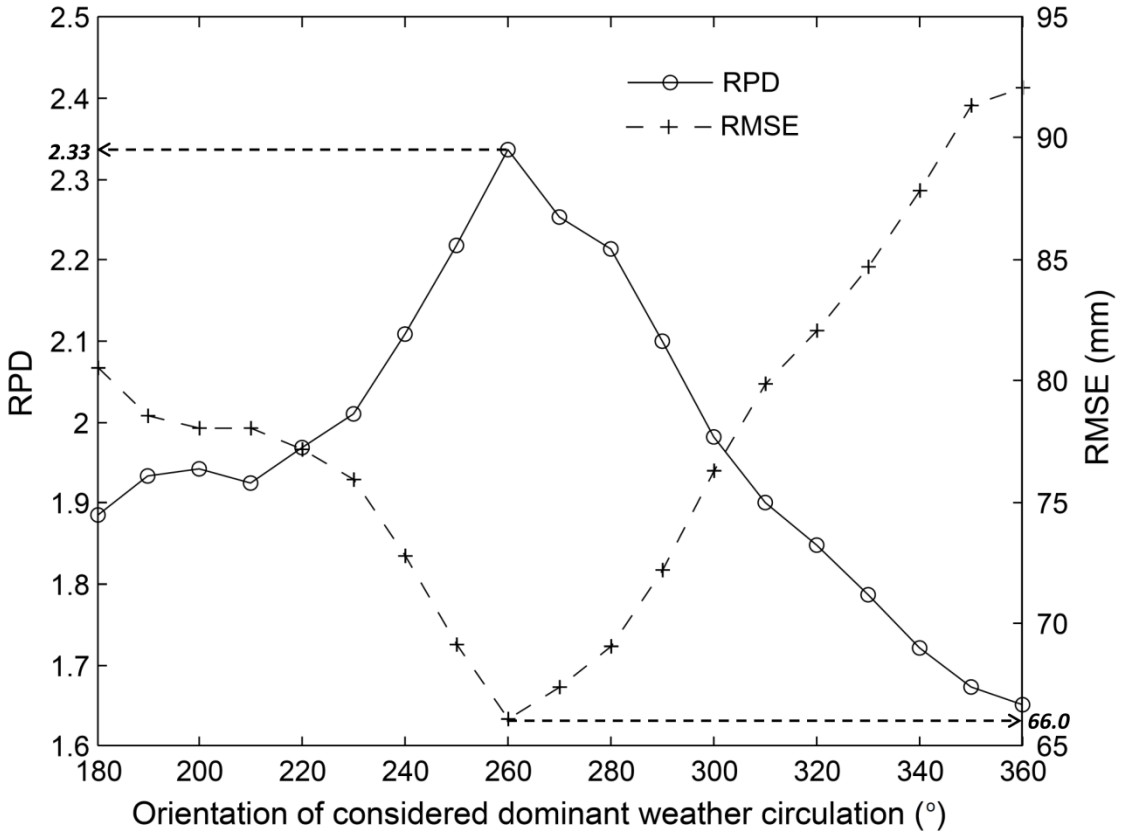

599

600 Figure 5: Root Mean Square Error (RMSE, mm) and Ratio of Performance to Deviation (RPD) of the

601 best model fit (R^2_{max}) in function of orientation of dominant weather circulation (°).

602

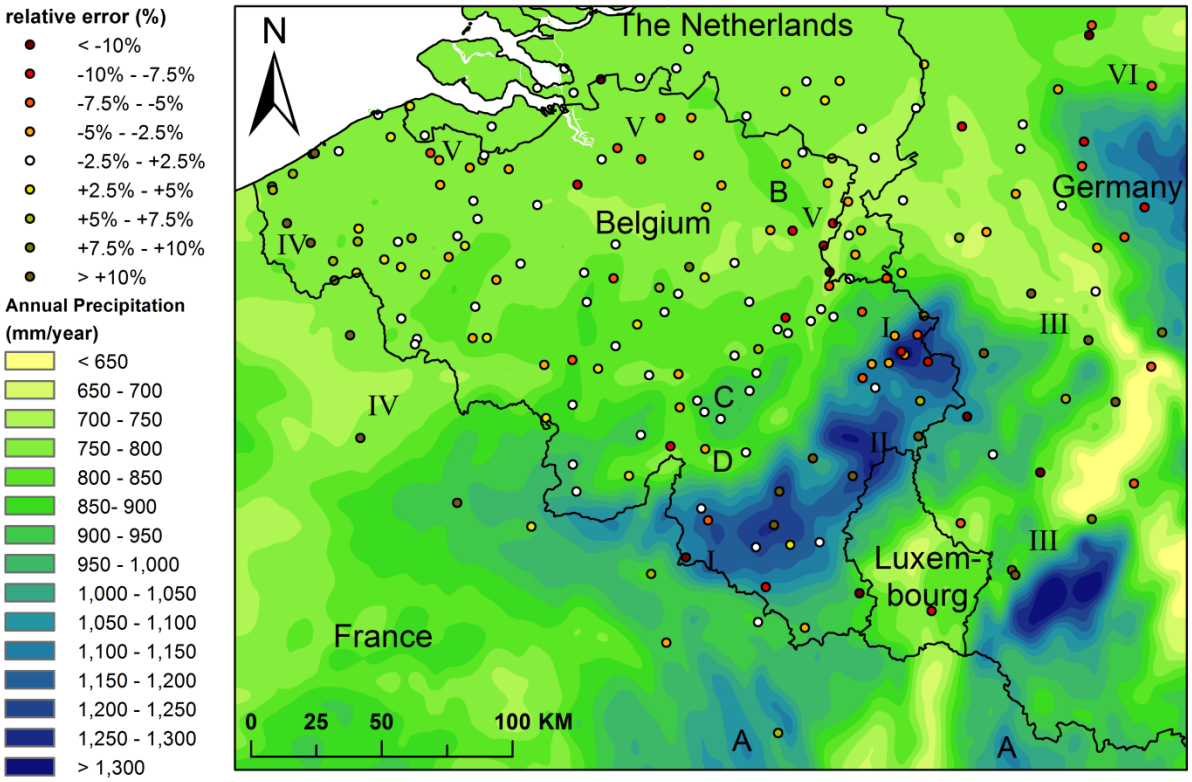

603

604

605 Figure 6: Estimated long term (1960-1990) total 30-year average annual precipitation map (mm yr^{-1})

606 for Belgium and surroundings with indication of relative error (%) at meteo-stations

607

608

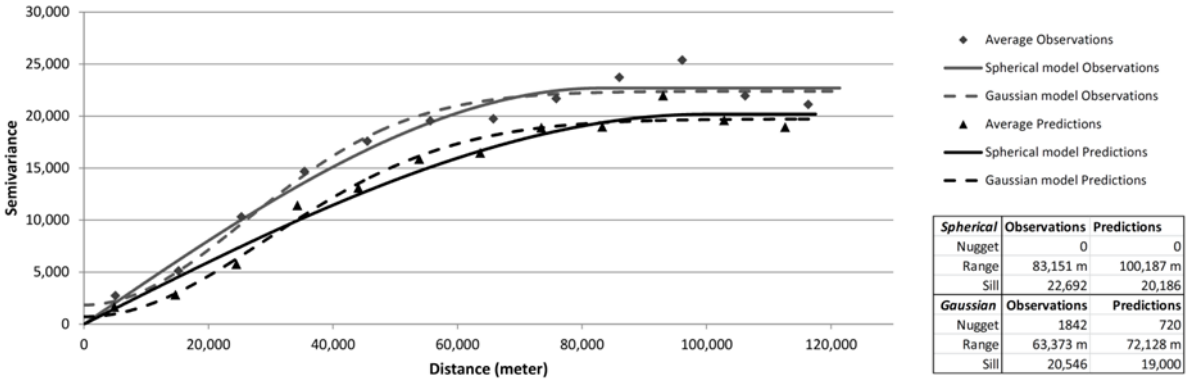

Spherical	Observations	Predictions
Nugget	0	0
Range	83,151 m	100,187 m
Sill	22,692	20,186
Gaussian	Observations	Predictions
Nugget	1842	720
Range	63,373 m	72,128 m
Sill	20,546	19,000

609 Figure 7: Semivariograms of the observed data (grey) versus predicted precipitation values (black).

610 The Spherical and Gaussian models as fitted through the averaged semivariance values and

611 associated nugget, range and sill values are obtained by using ARC-GIS' Geostatistical Wizard tool.

612

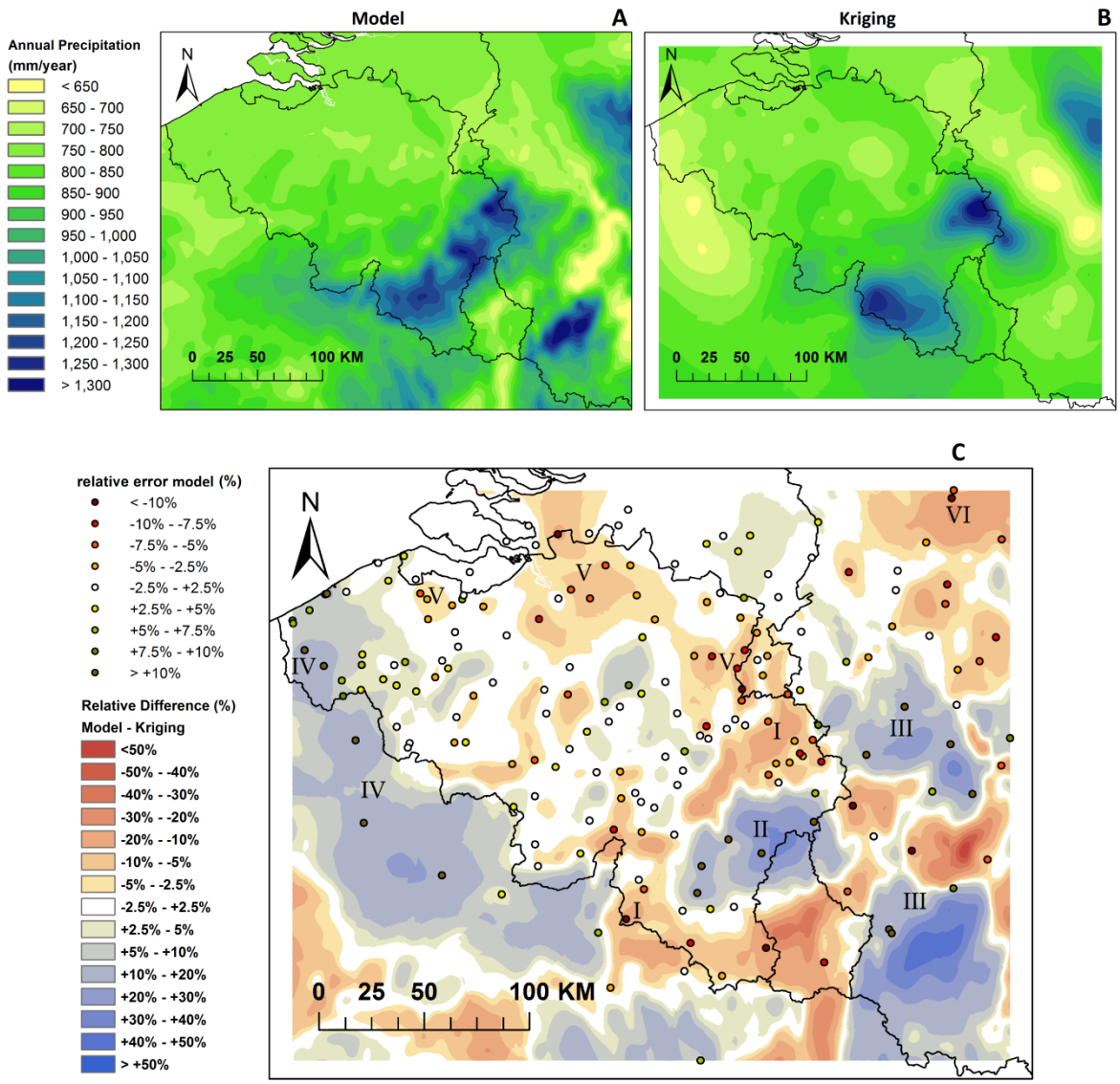

613

614 Figure 8: Subpanel A & B are showing precipitation maps as obtained by the presented approach and

615 the Ordinary Kriging, respectively. Subpanel C shows the relative difference between A and B,

616 including the relative error of the model as presented in fig. 6

617

618 Tables:

619

Parameter	Value	95% confidence interval	
a	1.3309	1.4269	1.2348
b	-0.0115	-0.0100	-0.0130
c	777.16	790.73	763.59

620

621 Table 1: Estimated parameter values of the selected model (i.e. resolution of H1 = 8.1 km, H2 = 90

622 km, S = 30.6 km, and orientation of dominant weather circulation (ODWC) of 260°)

623

624

			Resolution		
Rank	R2	ODWC (°)	H1 (km)	H2 (km)	S (km)
1	0.8192	260	8.1	90.0	30.6
2	0.8187	260	8.1	90.0	27.0
3	0.8186	270	8.1	94.5	27.0
4	0.8181	260	8.1	94.5	30.6
5	0.8179	270	8.1	94.5	30.6
6	0.8178	260	8.1	94.5	27.0
7	0.8155	270	8.1	99.0	27.0
8	0.8155	260	8.1	68.4	30.6
9	0.8154	260	7.2	90.0	30.6
10	0.8149	270	7.2	94.5	30.6

Table 2: Top 10 best model runs ranked following R^2 with annotation of the "Orientation of the dominant weather circulation" (ODWC) and aggregation resolution of smoothed model input maps (H1, H2 and S (eq. 1)).